ISBN: 978-3-95450-232-5 ISSN: 2673-7000 doi:10.18429/JACoW-NAPAC2022-TUPA21

HYDRODYNAMIC AND BEAM DYNAMIC SIMULATIONS OF ULTRA-LOW EMITTANCE WHOLE BEAM DUMPS IN THE ADVANCED PHOTON SOURCE STORAGE RING*

J. Dooling†, Y. Lee, M. Borland, A. Grannan, C. Graziani, R. Lindberg, G. Navrotski
Argonne National Laboratory, Lemont, IL 60439, USA
N. Cook, RadiaSoft, Boulder, CO 80301, USA
D. Lee, University of California, Santa Cruz, CA 95064, USA

Abstract

The Advanced Photon Source Upgrade will use a multi-bend achromatic lattice to reduce vertical and horizontal beam emittances by one- and two-orders of magnitude, respectively; the operating current will increase by a factor of two. The resulting electron beam will be capable of depositing more than 150 MGy on machine protection collimators creating high-energy-density conditions. Work is underway to couple the beam dynamics code `elegant` with the particle-matter interaction program MARS and the magnetohydrodynamics (MHD) code FLASH to model the effects of whole beam aborts on the collimators. Loss distributions from `elegant` are input to MARS, which provides dose maps to FLASH. We are examining MHD effects as well as the propagation of beam downstream after interacting with a collimator. Electron and positron components are tracked to determine locations of beam loss. In recent beam dump experiments, dose levels as high as 30 MGy were generated and resulted in severe damage to the collimator surfaces. The deformed collimator surface may lead to beam deposition in unexpected locations. A fan-out kicker will be used to mitigate the effects of whole beam dumps on the collimators.

INTRODUCTION

Particle-matter interaction simulations were conducted with MARS [1,2], which takes beam-dynamics loss distributions generated by `elegant` [3,4] as input. In this simulation study, it is indicated that the ultra-low emittance electron beams expected in the Advanced Photon Source Upgrade (APS-U) storage ring would damage most commonly used vacuum materials such as aluminum, titanium, copper, or tungsten.

Two irradiation experiments were carried out in the APS storage ring (SR) to assess the effects of high-intensity electron beams when the beam strikes the proposed collimator material for the APS-U [5]. These experiments indicated that high-energy-density (HED) conditions ($>10^{11}$J/m^3) [6] are generated in the struck material leading to significant damage. This data has been used to benchmark our simulations thus far, with good results overall.

Electron loss distributions from `elegant` are used as input to MARS to calculate energy deposition (or dose) in the collimator material. Dose maps from MARS are, in turn, passed to FLASH [7–9] to solve magnetohydrodynamic evolution using the unsplit staggered mesh (USM) MHD solvers [10, 11]. The propagation of the beam after interaction with the collimator is a prime concern. Experimental data, as well as simulations, clearly indicate that rapid, unplanned whole-beam loss erodes the collimator surface. Therefore, we want to track the beam and shower components downstream of the collimator during a whole-beam loss event. The beam carries a significant magnetic field with it, but as such, the field is transitory.

MAGNETOHYDRODYNAMICS

After resolving issues with the hydrodynamic solver [12], attention has turned to the inclusion of magnetohydrodynamic (MHD) effects. In MHD mode, magnetic fields in FLASH are not self-starting; henceforth none would be present without an externally-applied field (i.e., from the bunch). The FLASH simulation approximates initial boundary conditions at the vacuum-collimator interface using image charges in a reasonably correct way. Unfortunately, this model is no longer accurate after the boundary begins to erode.

We can calculate the electromagnetic fields near an electron beam by directly summing the field contributions from all electrons. A single relativistic electron produces the transverse electric field

$$\mathbf{E}_\perp(x,y,z,t) = \frac{e}{2\pi\epsilon_0}\frac{x\hat{\mathbf{x}}+y\hat{\mathbf{y}}}{\gamma^2\left[\frac{(x^2+y^2)}{\gamma^2}+(z-\beta ct)^2\right]^{3/2}}, \quad (1)$$

and the transverse magnetic field is $\mathbf{B}_\perp = (\beta/c)\hat{\mathbf{z}}\times\mathbf{E}_\perp$. We consider the field from a collection of N_e relativistic electrons whose coordinates are described by the probability distribution function f. We further assume that the electron distribution function varies in the longitudinal direction over the characteristic length σ_z, and that we are interested in transverse distances such that $r^2 \ll \gamma^2\sigma_z^2$. In this case, the field part of the integrand is a sharply peaked function which we can approximate by a delta function (see, e.g., Refs. [13, 14]).

* This research used resources of the Advanced Photon Source, a U.S. Department of Energy (DOE) Office of Science user facility and is based on work supported by Laboratory Directed Research and Development (LDRD) funding from Argonne National Laboratory, provided by the Director, Office of Science, of the U.S. DOE under Contract No. DE-AC02-06CH11357.
† dooling@anl.gov

ISBN: 978-3-95450-232-5 ISSN: 2673-7000 doi:10.18429/JACoW-NAPAC2022-TUPA21

Taking the ultra-relativistic limit and summing over all electrons implies that the field is given by

$$\mathbf{E}_\perp(x,y,z) = \frac{eN_e}{2\pi\epsilon_0}\int dx'dy'dz'\; f(x',y',z-ct) \times \frac{(x-x')\hat{\mathbf{x}}+(y-y')\hat{\mathbf{y}}}{(x-x')^2+(y-y')^2}. \tag{2}$$

Hence, in the ultra-relativistic limit, the result is independent of γ, as we would expect. Furthermore, the field is given by the convolution of f with what is essentially the 2D Green function of the electric field.

To make further progress, we next assume that the distribution function is separable into its longitudinal and transverse components. In this case, the field along any transverse plane is essentially that of a 2D source associated with the local line density. Hence, for a storage ring where f is Gaussian in all three planes, the field is proportional to that calculated by Bessetti and Erskine [15]:

$$E_x - iE_y = \frac{ieN_e e^{-(z-ct)^2/2\sigma_z^2}}{4\pi\epsilon_0\sigma_z\sqrt{\sigma_x^2-\sigma_y^2}}\left[w\left(\frac{x+iy}{\sqrt{2(\sigma_x^2-\sigma_y^2)}}\right) - e^{-x^2/2\sigma_x^2}e^{-y^2/2\sigma_y^2}w\left(\frac{\Upsilon x+iy/\Upsilon}{\sqrt{2(\sigma_x^2-\sigma_y^2)}}\right)\right], \tag{3}$$

where the ratio $\Upsilon = \sigma_y/\sigma_x$, while the complex error/Faddeeva function is defined by

$$w(z) = e^{-z^2}\left(1+\frac{2i}{\sqrt{\pi}}\int_0^z d\zeta\; e^{\zeta^2}\right). \tag{4}$$

For the APS we have $1/2 \gtrsim \Upsilon \gtrsim 1/20$ and Eq. (3) must be used. On the other hand, in the APS-U the beam can be round, $\sigma_x = \sigma_y$ and $\Upsilon = 1$, in which case we can apply the considerably simpler

$$E_x - iE_y = \frac{eN_e e^{-\frac{(z-ct)^2}{2\sigma_z^2}}}{(2\pi)^{3/2}\epsilon_0\sigma_z}\frac{x-iy}{x^2+y^2}\left[1-e^{-\frac{(x^2+y^2)}{2\sigma_x^2}}\right]. \tag{5}$$

For any electron beam with $\Upsilon \leq 1$, the field reaches its maximum value along the line $x = 0$ and $z = ct$. We plot the predicted vertical field E_y for a total charge $q = 15.3$ nC and along this line in Fig. 1. The left-hand plot assumes that $\sigma_x = 170$ microns, $\sigma_z = 10$ mm, and $\Upsilon = 0.085$, and is representative of the present APS, while the right-hand plot uses a round beam ($\Upsilon = 1$) with $\sigma_x = 12$ microns and $\sigma_z = 30$ mm as may be the case in the APS-U. We see that the peak fields in each case are around 65 MV/m and 140 MV/m, respectively.

In addition to the beam fields themselves, we expect that the image currents along the chamber surface will contribute as the beam approaches the wall. If the chamber is metal and the distance between the chamber and the beam is much smaller than the chamber's radius, we can approximate the wall as a flat, perfect conductor. In this case, the fields outside the wall can be found using the method of images, where

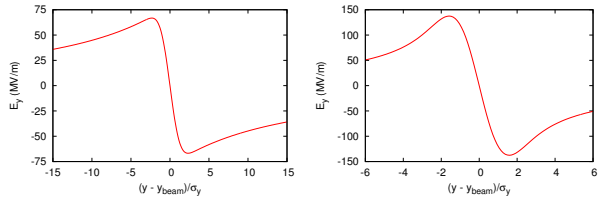

Figure 1: Maximum space-charge field E_y in the lab frame for $q = 15.3$ nC and a flat beam at the APS (left, with $\sigma_x = 170$ microns, $\sigma_z = 10$ mm, and $\Upsilon = 0.85$), and a round beam at the APS-U (right, with $\sigma_x = 12$ microns and $\sigma_z = 30$ mm.).

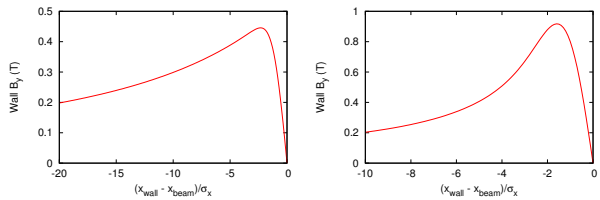

Figure 2: Maximum magnetic field B_y along the wall for the same parameters as Fig. 1 including the image fields which effectively double B_y.

the (fictitious) image charges are effectively a reflection of the electron beam in the plane of the chamber wall with an opposite charge. This cancels the transverse component of the field while doubling the perpendicular component. Likewise, the axial component of the magnetic field parallel to the wall is doubled. We plot the resulting magnetic field along the wall at $x = x_{\rm wall}$ in Fig. 2.

A contour plot of the magnetic field intensity for the round beam case, including the image currents, is presented in Fig. 3 with the beam centroid 100 microns from the collimator boundary. Note that intensity values for $x < -4.2$ mm are fictitious. These fields are present only with the electron bunch. At the boundary, the magnetic field is entirely in the y-direction to satisfy the boundary conditions for the image current density, $\mathbf{J}_s = \hat{\mathbf{n}} \times \mathbf{H}$, where $\hat{\mathbf{n}}$ is the surface normal and $\mathbf{H}$ is the magnetic field.

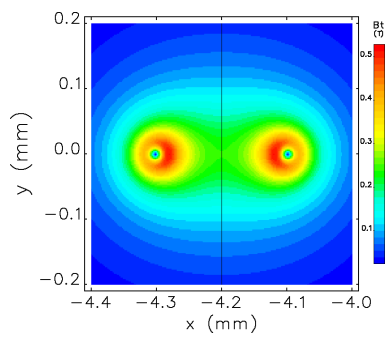

Figure 3: Transverse magnetic field intensity contours for the round beam case of Fig. 1, but also including the image fields. The collimator-vacuum boundary occurs at $x = 4.2$ mm. Intensity values for $x < -4.2$ mm are fictitious.

ISBN: 978-3-95450-232-5 ISSN: 2673-7000 doi:10.18429/JACoW-NAPAC2022-TUPA21

TIME-VARYING DOSE

For initial FLASH simulations, the total dose map was determined from `elegant` loss distributions based either on experimental data or the APS-U model. The dose distribution was then divided equally over all bunches in a beam dump. For example, in an experiment-based, 200-mA case with a 972-bunch fill pattern, both simulation and experiment indicated that the full width at half maximum (FWHM) loss duration takes approximately three turns (one turn= 3.68 µs); therefore, the total dose map was divided by 2916 and applied repetitively over three turns. Simulated and measured loss intensity waveforms are plotted in Fig. 4. Elegant simulations provide temporal loss variation turn-by-turn. We are presently using the five largest PassCount values displayed in Fig. 4 as input to FLASH to determine collimator behavior.

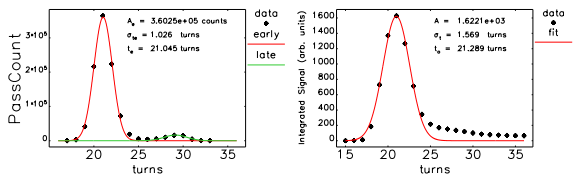

Figure 4: 200 mA loss distribution with Gaussian fits to the respective peaks; (left) `elegant`-derived, (right) loss monitor signal.

The total accumulated x-y dose map generated by MARS over all turns using the `elegant` loss distribution of the 202 mA, 6 GeV beam dump case shown in Fig. 4 is given in Fig. 5. The location $x = -0.2$ cm represents the boundary between the collimator to the left and the vacuum to the right.

Collimator behavior, when subjected to this uniform 202-mA irradiation, is presented in Fig. 6. The release condition, where solid material is converted into plasma, is $1.5T_{\mathrm{vap}}$ where T_{vap} is the vaporization temperature. For aluminum, T_{vap}=2743 K. The boundary between solid and plasma regions is indicated by the white curve in Fig. 6; the black regions are locations where the temperature exceeds aluminum's melting temperature, $T_{\mathrm{m}} = 933$ K.

DOWNSTREAM PROPAGATION

Only a fraction of the beam energy is deposited in the collimator. The majority of the energy is in the form of scattered electrons and electromagnetic shower components, which continue downstream. Electron and positron trajectories after the collimator are recorded and used as input to `elegant` for tracking downstream. The population of each species is tallied as a function of longitudinal orbit coordinate s and plotted in Fig. 7. In this case, erosion of the collimator surface has not been included. As might be expected, the positrons do not travel far, whereas the electron component is lost mainly at the first insertion device vacuum chamber approximately 100 m downstream of the collimator.

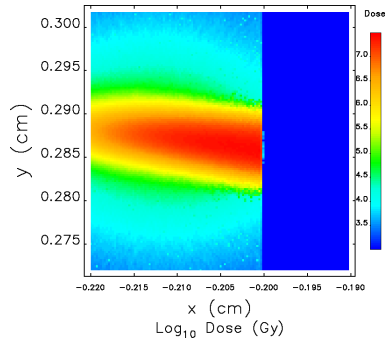

Figure 5: Total dose map of the 202 mA, 6 GeV beam dump shown in Fig. 4; contours are plotted on log scale.

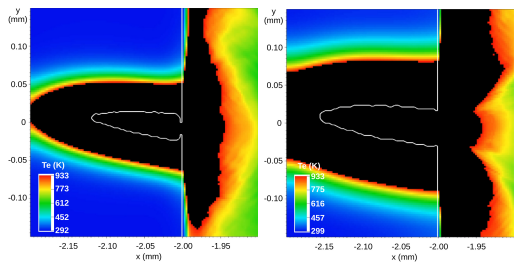

Figure 6: FLASH temperature maps and release boundary at the collimator apex after one and three turns with 200 mA, 6 GeV electron beam irradiation. Black regions at locations where $x < -2.0$ mm or less than the boundary are areas with temperatures above 933 K that have not yet been released to the plasma state.

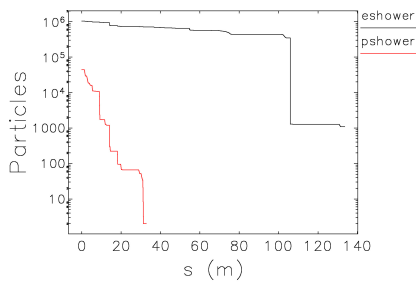

Figure 7: Trajectory count downstream of the collimator after a beam strike.

SUMMARY

We provided a description of external magnetic fields generated by a bunch. Although promising, this model is only accurate before the beam impacts the surface. Downstream propagation of the shower is likely to be modified by the trench carved out by the beam. For our future work, we are coupling density maps from FLASH back to MARS and `elegant` to provide a more accurate picture of the dynamics of whole-beam dumps in fourth generation storage-rings.

ACKNOWLEDGEMENTS

Thanks to R. Soliday and H. Shang for assistance with analysis scripts.

ISBN: 978-3-95450-232-5 ISSN: 2673-7000 doi:10.18429/JACoW-NAPAC2022-TUPA21

REFERENCES

[1] N. V. Mokhov, "The mars code system user's guide", Fermilab, USA, Rep. FN 628, 1995.

[2] N. V. Mokhov and S. I. Striganov, "MARS15 Overview", in *AIP Conf. Proc.*, vol. 896, no. 1, pp. 50–60, 2007. doi:10.1063/1.2720456

[3] M. Borland, "elegant: A flexible sdds-compliant code for accelerator simulation", Advanced Photon Source, USA, Tech. Rep. LS-287, Sep. 2000.

[4] Y. Wang and M. Borland, "Implementation and Performance of Parallelized Elegant", in *Proc. PAC'07*, Albuquerque, NM, USA, Jun. 2007, paper THPAN095, pp. 3444–3446.

[5] J. Dooling *et al.*, "Collimator irradiation studies in the argonne advanced photon source at energy densities expected in next-generation storage ring light sources", *Phys. Rev. Accel. Beams*, vol. 25, no. 4, p. 043001, Apr. 2022. doi:10.1103/PhysRevAccelBeams.25.043001

[6] R. P. Drake, *High-Energy-Density Physics, Foundation of Inertial Fusion and Experimental Astrophysics, Second Edition*. Berlin, Germany: Springer, 2018.

[7] B. Fryxell *et al.*, "FLASH: An adaptive mesh hydrodynamics code for modeling astrophysical thermonuclear flashes", *Astrophys. J. Suppl. Ser.*, vol. 131, no. 1, pp. 273–334, Nov. 2000. doi:10.1086/317361

[8] A. Dubey *et al.*, "Evolution of flash, a multi-physics scientific simulation code for high-performance computing", *Int. J. High Perform. Comput. Appl.*, vol. 28, no. 2, pp. 225–237, May 2014. doi:10.1177/1094342013505656

[9] A. Dubey *et al.*, "Ongoing verification of a multiphysics community code: Flash", *J. Software: Pract. Exper.*, vol. 45, no. 2, pp. 233–244, 2015. doi:10.1002/spe.2220

[10] D. Lee and A. E. Deane, "An unsplit staggered mesh scheme for multidimensional magnetohydrodynamics", *J. Comput. Phys.*, vol. 228, no. 4, pp. 952–975, 2009. doi:10.1016/j.jcp.2008.08.026

[11] D. Lee, "A solution accurate, efficient and stable unsplit staggered mesh scheme for three dimensional magnetohydrodynamics", *J. Comput. Phys.*, vol. 243, pp. 269–292, 2013. doi:10.1016/j.jcp.2013.02.049

[12] J. C. Dooling *et al.*, "Simulations of Beam Strikes on Advanced Photon Source Upgrade Collimators using FLASH, MARS, and elegant", in *Proc. IPAC'21*, Campinas, Brazil, May 2021, pp. 2562–2565. doi:10.18429/JACoW-IPAC2021-WEXC04

[13] A. W. Chao, *Physics of Collective Beam Instabilities in High Energy Accelerators*. New York, USA: Wiley, 1993.

[14] G. Stupakov, "Wakefields and Collective Beam Instabilities", USPAS, Jan. 2019.

[15] M. Bassetti and G. Erskine, "Closed expression for the electrical field of a two-dimensional gaussian charge", CERN, Geneva, Switzerland, Rep. CERN-ISR-TH/80-06 80-06, 1980.